

Structural characterization of the mitomycin 7-*O*-methyltransferase

Shanteri Singh,¹ Aram Chang,² Randal D. Goff,¹ Craig A. Bingman,² Sabine Grüşchow,^{3,4} David H. Sherman,^{3,4} George N. Phillips Jr.,^{2*} and Jon S. Thorson^{1*}

¹ Division of Pharmaceutical Sciences, Wisconsin Center for Natural Product Research, School of Pharmacy, University of Wisconsin-Madison, Madison, Wisconsin 53705

² Department of Biochemistry, University of Wisconsin-Madison, Madison, Wisconsin 53706

³ Life Sciences Institute, University of Michigan, Ann Arbor, Michigan 48109-2216

⁴ Department of Medicinal Chemistry, University of Michigan, Ann Arbor, Michigan 48109-2216

ABSTRACT

Mitomycins are quinone-containing antibiotics, widely used as antitumor drugs in chemotherapy. Mitomycin-7-*O*-methyltransferase (MmcR), a key tailoring enzyme involved in the biosynthesis of mitomycin in *Streptomyces lavendulae*, catalyzes the 7-*O*-methylation of both C9 β - and C9 α -configured 7-hydroxymitomycins. We have determined the crystal structures of the MmcR–*S*-adenosylhomocysteine (SAH) binary complex and MmcR–SAH–mitomycin A (MMA) ternary complex at resolutions of 1.9 and 2.3 Å, respectively. The study revealed MmcR to adopt a common *S*-adenosyl-L-methionine-dependent *O*-methyltransferase fold and the presence of a structurally conserved active site general acid–base pair is consistent with a proton-assisted methyltransfer common to most methyltransferases. Given the importance of C7 alkylation to modulate mitomycin redox potential, this study may also present a template toward the future engineering of catalysts to generate uniquely bioactive mitomycins.

Proteins 2011; 79:2181–2188.
© 2011 Wiley-Liss, Inc.

Key words: methyltransferase; natural product; mitomycin; biosynthesis; *S*-adenosyl-L-methionine; cancer; X-ray crystallography.

INTRODUCTION

Originally discovered over six decades ago,^{1–3} the natural product mitomycin C [MMC, Fig. 1(A)] remains part of the conventional anticancer regimen for solid tumors given its bias toward hypoxia-induced cytotoxicity.^{4–7} Numerous bioreductants have been implicated in MMC activation via one- or two-electron reduction of the quinone, including nicotinamide adenine dinucleotide (NADPH)/cytochrome P450 reductase, NADPH:quinone oxidoreductase (DT-diaphorase), and/or glutathione. Under oxygen-limiting conditions, one-electron reduction predominates, producing a highly reactive quinone methide that alkylates DNA.^{4,5} However, certain MMC-activating agents operate under both anaerobic and aerobic conditions [e.g., NADPH:quinone oxidoreductase (DT-diaphorase)] and can thereby compromise the hypoxic selectivity of quinone-alkylating agents such as MMC.⁶ The reactivity, as well as corresponding cytotoxic selectivity, correlates in part to the redox potential of the quinone ring, which, in turn, can be modulated via appended functional groups. Modifications at the C6 and C7 positions, achieved through derivatization of naturally occurring mitomycins, provide further support for this notion.⁴ Thus, understanding the structural basis for enzymes involved in mitomycin C6 or C7, alkylation may enable the exploitation of these catalysts toward the generation of new and improved mitomycin analogs.

Metabolic labeling studies revealed D-glucosamine and 3-amino-5-hydroxybenzoic acid to be the biosynthetic precursors of the mitosane skeleton, the C-10 carbamoyl group to derive from L-arginine or L-citrulline, and the *N*- and *O*-methyl moieties to originate from L-methionine.^{8–11} Based on annotation of the mitomycin biosynthetic gene cluster from *Streptomyces lavendulae* Agricultural Research Service Culture Collection (NRRL) 2564 [producer of mitomycins A–C; Fig. 1(A)],¹² there exist three *S*-adenosyl-L-methionine

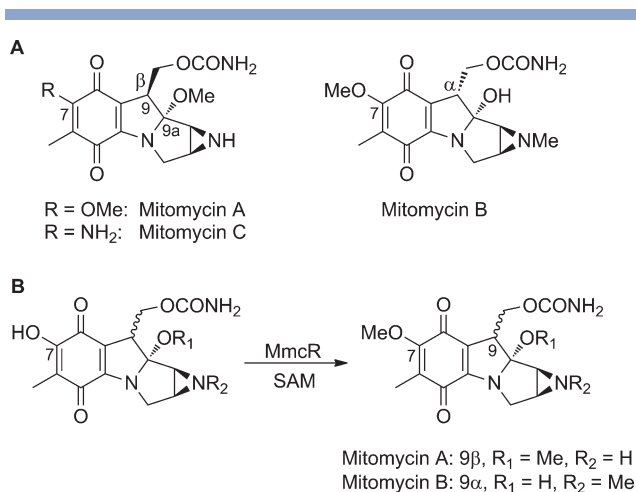
Additional Supporting Information may be found in the online version of this article.

Grant sponsor: NIH; Grant number: CA84374; Grant sponsor: National Cancer Institute; Grant number: Y1-CO-1020; Grant sponsor: National Institute of General Medical Science; Grant number: Y1-GM-1104; Grant sponsor: Center for Eukaryotic Structural Genomics (NIH); Grant number: GM074901s; Grant sponsor: U.S. Department of Energy, Basic Energy Sciences, Office of Science; Grant number: W-31-109-ENG-38; Grant sponsors: Laura and Edward Kremers Chair in Natural Products Chemistry, Michigan Technology Tri-Corridor, Michigan Economic Development Corporation

*Correspondence to: George N. Phillips Jr., Department of Biochemistry, University of Wisconsin-Madison, Madison, WI 53706. E-mail: phillips@biochem.wisc.edu or Jon S. Thorson, Division of Pharmaceutical Sciences, Wisconsin Center for Natural Product Research, School of Pharmacy, University of Wisconsin-Madison, Madison, WI 53705. E-mail: jsthorson@pharmacy.wisc.edu

Received 2 December 2010; Revised 9 February 2011; Accepted 19 February 2011

Published online 22 March 2011 in Wiley Online Library (wileyonlinelibrary.com). DOI: 10.1002/prot.23040

**Figure 1**

(A) Naturally occurring mitomycins. (B) The reaction catalyzed by MmcR.

(SAM)-dependent methyltransferase-encoding genes in the mitomycin gene cluster.¹³ Of the corresponding proteins, MmcR shows high sequence similarity to natural product phenolic methyltransferases (MTases) such as bacterial MTases involved in the biosynthesis of calicheamicin, dynemicin, C-1027, fredericamycin, oxytetracycline, puromycin, and plant MTases involved in the biosynthesis of flavonoids. Recent MmcR *in vivo* and *in vitro* studies have revealed MmcR to catalyze the efficient methylation of 7-demethylmitomycin A and 7-desmethylmitomycin B [Fig. 1(B)] over a broader pH range in a metal-independent manner.¹⁴ Although MmcR was demonstrated to tolerate both C9 α - and C9 β -configurations *in vitro*, the enzyme displays a strong preference for the C9 β -isomer.¹⁴ In an effort to further our understanding of the mechanism of MmcR catalysis and the key structural elements for SAM recognition and activation, herein, we report the crystal structures of the MmcR–S-adenosylhomocysteine (SAH) binary complex and MmcR–SAH–mitomycin A (MMA) ternary complex at resolutions of 1.9 and 2.3 Å, respectively. This work reveals MmcR to crystallize as a dimer and to adopt a fairly typical MTase structural fold. Given the ability of structurally homologous DNA- and natural product-MTases to use non-natural cofactor analogs of SAM to achieve differential alkylation,^{15–22} this study supports the notion that MmcR (in conjunction with SAM surrogates) may also present an opportunity to further modulate the redox potential of mitomycin.

MATERIALS AND METHODS

Mitomycin A synthesis

Mitomycin C (109 mg, 0.326 mmol) was suspended in an aqueous solution of NaOH (0.05M, 8 mL) under Ar at

room temperature and was excluded from light. After stirring for 16 h, the sodium mitosane salt ($R_f = 0.08$, 10% MeOH in CH₂Cl₂) was cooled to 0°C and acidified to a pH of 3.9 with 0.1M H₂SO₄. The aqueous solution was extracted with EtOAc (4 × 10 mL) and then dried with Na₂SO₄. Evaporation of the solvent yielded the hydroxymitosane as a purple solid (95 mg). Methylation was performed by first dissolving the solid in tetrahydrofuran (THF) (20 mL) and cooling to 0°C, and then slowly adding an ethereal solution of diazomethane (20 mL; prepared by adding 250 mg of *N*-methyl-*N'*-nitro-*N*-nitrosoguanidine to 20 mL of 40% aqueous KOH and 20 mL Et₂O). The reaction proceeded for 10 min at 0°C and was quenched with HOAc (250 μ L). After removing the solvent, the residue was purified by column chromatography (SiO₂, 5% MeOH in CH₂Cl₂) providing mitomycin A as an amorphous solid (43 mg, 43%, TLC, $R_f = 0.51$, 10% MeOH in CH₂Cl₂). ¹H NMR (acetone-*d*₆, 500 MHz) δ 5.94 (br s, 2H), 4.72 (dd, $J = 10.6$, 4.4 Hz, 1H), 4.30 (t, $J = 10.6$ Hz, 1H), 4.02 (s, 3H), 3.93 (d, $J = 12.5$ Hz, 1H), 3.51 (dd, $J = 11.0$, 4.4 Hz, 1H), 3.42 (d, $J = 12.1$ Hz, 1H), 3.21 (s, 3H), 2.90 (br s, 1H), 2.84 (br s, 1H), 1.79 (s, 3H); ¹³C NMR (acetone-*d*₆, 125 MHz) δ 184.3, 179.7, 159.3, 158.4, 153.5, 125.3, 116.0, 108.3, 63.5, 62.5, 51.8, 50.8, 45.9, 38.2, 34.3, 9.2; HRMS (ESI) m/z C₁₆H₁₉N₃NaO₆ ([M+Na]⁺) 372.1171, calculated 372.1166.

Protein expression and purification

Recombinant *N*-His₆-MmcR (herein, referred to simply as MmcR) was produced in *Escherichia coli* and affinity purified as previously described.¹⁴ The purified enzyme in 20 mM Tris, pH 8, 50 mM NaCl was subsequently concentrated to 20 mg/mL, drop frozen in liquid nitrogen, and stored at –80°C. Protein concentrations were determined by Bradford assay (Bio-Rad, Hercules, CA) using bovine serum albumin (BSA) as a standard. For the production of selenomethionine (SeMet)-labeled protein, the *E. coli* methionine auxotroph strain B834 (DE3) was transformed with plasmid *N*-His₆-*mmcR*¹⁴ and the production of the desired (SeMet)-labeled recombinant protein accomplished using autoinduction media.²³

Protein crystallization

Crystals of MmcR with SAH were grown by vapor diffusion in hanging drops containing a 1:1 mixture of 1 μ l protein and 1 μ l crystallization buffer [10% (w/v) polyethylene glycol 4000, 15% 2-methyl-2,4-pentadiol (MPD), 100 mM CaCl₂, and 100 mM 2-(*N*-morpholino)ethanesulfonic acid (MES) (pH 6.0) at 4°C]. Crystals of MmcR in complex with MMA were obtained by soaking the MmcR–SAH crystals in the crystallization solution with 5 mM MMA for 8 h. Diffraction data were collected from a single crystal that was soaked in crystallization solution containing 25% ethylene glycol, mounted

in a cryoloop and flash frozen in a stream of liquid nitrogen.

MmcR structure determination

All diffraction data for SeMet-labeled MmcR–SAH complexes were collected at the General Medicine and Cancer Institute Collaborative Access Team (GM/CA-CAT) 23-ID-D beamline at the Advanced Photon Source of Argonne National Laboratory. Each of the 180 diffraction images for the SeMet-labeled crystals was collected at a crystal-to-detector distance of 270 mm, exposed for 5 s, in a single pass with 1° oscillation per frame. Data sets for the MmcR–SAH complex were collected at two wavelengths: 0.97945 and 0.96421 Å. The diffraction images were indexed, integrated, and scaled using HKL2000.²⁴ Diffraction data for SeMet-labeled MmcR–SAH–MMA complexes were collected at the Life Science Collaborative Access Team (LS-CAT) 21-ID-F beamline at the Advanced Photon Source of Argonne National Laboratory. Each of the 120 -diffraction images for the SeMet-labeled crystals was collected at the crystal-to-detector distance of 225 mm, exposed for 4 s, in a single pass with 1° oscillation per frame and at 0.97872 Å wavelength. The diffraction images were indexed, integrated, and scaled using HKL2000. Both complexes crystallized in space group $P2_12_12_1$ with four molecules per asymmetric unit. Unit cell dimensions for MmcR–SAH were $a = 88.3$ Å, $b = 98.9$ Å, and $c = 171.1$ Å and for MmcR–SAH–MMA were $a = 87.8$ Å, $b = 98.8$ Å, and $c = 171.0$ Å.

Phases for the MmcR–SAH complex were determined using the multiple wavelength anomalous dispersion method on SeMet-substituted protein. Initial heavy atom sites were found using the programs PHENIX.HySS²⁵ and SHELXD.^{26,27} PHENIX.EMMA identified 16 consensus sites. The structure was automatically phased, and density modification was performed using auto-SHARP.²⁸ Using the initial phase information, a high-resolution model of MmcR–SAH was built in ARP/wARP.²⁹ Using the MmcR–SAH structure as a search model, the MmcR–SAH–MMA structure was obtained by molecular replacement using MOLREP.³⁰ The structure was completed via multiple manual interactions in COOT³¹ followed by refinement in REFMAC5³² and PHENIX.Refine.³³ The quality of all models was assessed using the program MOLPROBITY³⁴ and PROCHECK.³⁵ The final model of MmcR–SAH contained residues 11–349 in each of the 4 monomers, 871 water molecules, 4 molecules of SAH, and MPD. The MmcR–SAH–MMA model contained residues 11–349, 329 water molecules, and 4 molecules of SAH and MMA. Topology and parameter files for SAH and MPD were obtained from the REFMAC library. Topology and parameter files for MMA were obtained by modifying the MMC structure with SKETCHER.³⁶ All figures are generated using molecular graphics program PyMOL. The binary and

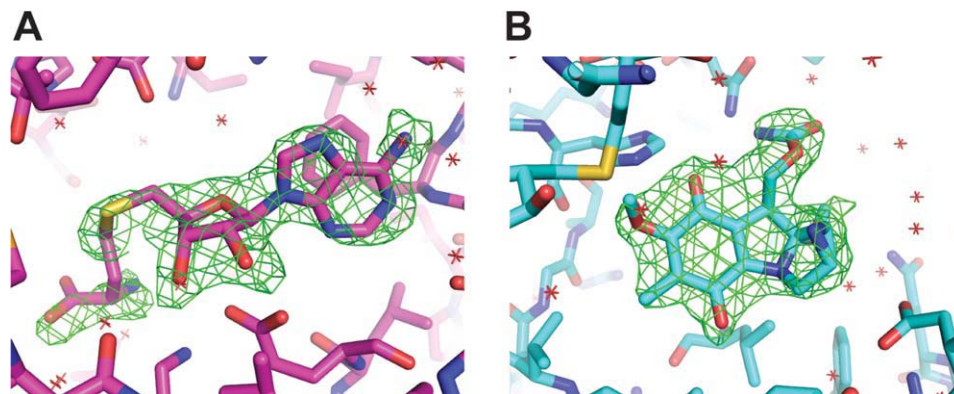
ternary complexes have been deposited under accession numbers 3GWZ and 3GXO, respectively.

RESULTS AND DISCUSSION

Recombinant MmcR, a 38-kDa protein consisting of 349 amino acids, was expressed in *E. coli* as N-terminal polyhistidine-tagged protein and purified by Ni^{2+} affinity chromatography. In the MmcR–SAH and MmcR–SAH–MMA binary and ternary complexes, the first 30 residues of chain A–D (20 residues of which comprised the N-terminal His-tag in each case) were not modeled due to insufficient electron density. The electron density for the rest of the polypeptide chain and the bound ligands is well defined [Fig. 2(A,B)]. The final structure was refined to an R_{cryst} and R_{free} of 17.4% and 21.0% for MmcR–SAH and 20.2% and 25.5% for MmcR–SAH–MMA complex, respectively (Table I).

Overview of the structure

Each subunit of MmcR exhibited a C-terminal catalytic domain and N-terminal dimerization domain. The C-terminal domain contains the conserved DXGXGXG fingerprint needed for cofactor binding. It is folded into a Rossmann fold, comprising a central parallel β -sheet ($\beta 1$ – $\beta 7$), where all except $\beta 7$ are parallel to each other and surrounded by seven alternating α -helices ($\alpha 10$ – $\alpha 16$) [Fig. 3(A)]. The sequence of secondary structural elements in this core SAM-binding domain is composed of $\alpha 10$, $\beta 1$, $\alpha 11$, $\beta 2$, $\alpha 12$, $\beta 3$, $\beta 4$, $\gamma 13$, $\alpha 14$, $\beta 5$, $\alpha 15$, $\alpha 16$, $\beta 6$, and $\beta 7$. The N-terminal domain involved in dimerization and for substrate binding contains all α -helical secondary structural elements. The secondary elements mainly engaged in dimer formation include the helices $\alpha 1$, $\alpha 4$, $\alpha 6$, $\alpha 7$, and $\alpha 15$ [Fig. 3(B)]. The interaction area of dimer interface is 3146 \AA^2 [Fig. 3(B)], mostly dominated by hydrophobic interactions along with 29 hydrogen bonds and 17 salt bridges. Analysis of crystal packing does not support the formation of a tetramer, as the interaction in the crystal lattice is rather weak. The largest interaction area with an adjacent molecule is only 467 \AA^2 , indicative of crystal contacts rather than a protein–protein interface. This is consistent with biochemical analysis by native sodium dodecyl sulfate/polyacrylamide gel electrophoresis (determined MW 73.2 kDa; calculated MW for the dimer, 75.2 kDa; data not shown). The MmcR-bound product (MMA) is situated at the interface of N- and C-terminal domains [Fig. 3(A)], and residues from both of these domains are involved in product binding. The fold of MmcR very much resembles previously reported O-MTases such as carminomycin 4-O-methyltransferase (DnrK),³⁷ neocarzinostatin O-methyltransferase (NcsB1),³⁸ chalcone O-methyltransferase (ChOMT),³⁹ isoflavone O-methyltransferase

**Figure 2**

Simulated annealing omit $F_o - F_c$ electron density maps contoured at 3σ . (A) Bound SAH and (B) bound MMA in MmcR-SAH-MMA ternary complex.

Table I

Crystal Parameters, X-ray Data Collection, Phasing, and Refinement Statistics

	MmcR-SAH		MmcR-SAH-MMA
Crystal parameters	Peak	HRem	
Space group	$P2_12_12_1$	$P2_12_12_1$	$P2_12_12_1$
Unit-cell parameters (\AA , $^\circ$)	$a = 88.3$, $b = 98.9$, $c = 171.1$	$a = 88.5$, $b = 99.0$, $c = 171.4$	$a = 87.8$, $b = 98.8$, $c = 171.0$
Data collection statistics			
Wavelength (\AA)	0.97945	0.96421	0.97872
Energy (eV)	12658.6	12858.6	12,668
Resolution range (\AA)	50.00–1.91 (1.98–1.91)	100.00–2.00 (2.07–2.00)	50.00–2.30 (2.38–2.30)
No. of reflections (measured/unique) ^a	220,672/115,235	194,218/101,748	708,974/59,548
Completeness (%)	98.6 (87.9)	98.8 (92.2)	88.8 (70.7)
R_{merge}^b	0.113 (0.570)	0.128 (0.903)	0.092 (0.315)
Redundancy	13.6 (9.2)	13.3 (9.3)	3.9 (3.3)
Mean $I/\sigma(I)$	11.5 (2.4)		11.3 (3.9)
Phasing statistics			
Mean FOM (centric/acentric)	0.090/0.322		
Phasing power (isomorphous/anomalous)	0.0/0.98		
Cullis R -factor (isomorphous/anomalous)	0.0/0.84		
Refinement and model statistics			
Resolution range	19.65–1.91 (1.93–1.91)		43.92–2.30 (2.38–2.30) ^d
No. of reflections (work/test)	114,971/5763		59,450/3003
R_{cryst}^e	0.174 (0.253)		0.202 (0.235)
R_{free}^f	0.210 (0.333)		0.255 (0.298)
RMSD bonds (\AA)	0.006		0.007
RMSD angles ($^\circ$)	1.000		1.102
ESU from R_{free}^g (\AA) ^g	0.23		0.19
B -factor—overall/waters (\AA^2) ^h	23.4/40.4		36.5/40.9
No. of protein molecules/all atoms	4/11428		4/10866
No. of waters	871		329
Ramachandran plot by MOLPROBITY (%)			
Favored regions	98.7		97.6
Additional allowed regions	1.2		2.4
Outliers	0.1		0.0
PBD code	3GWZ		3GXO

^aValues in parentheses are for the highest resolution shell.

^b $R_{\text{merge}} = \sum_i \sum_j |I_i(h) - \langle I(h) \rangle| / \sum_i \sum_j I_i(h)$, where $I_i(h)$ is the intensity of an individual measurement of the reflection and $\langle I(h) \rangle$ is the mean intensity of the reflection.

^cResolution range for phasing in SHARP was (26.66–3.2) \AA .

^dResolution range for refinement was cut (38.76–1.90) \AA due to low completeness and signal in the remaining resolution shells.

^e $R_{\text{cryst}} = \sum_j |F_{\text{obs}}| - |F_{\text{calc}}| / \sum_j |F_{\text{obs}}|$, where F_{obs} and F_{calc} are the observed and calculated structure-factor amplitudes, respectively.

^f R_{free} was calculated as R_{cryst} using ~5.0% of the randomly selected unique reflections that were omitted from structure refinement.

^gEstimated standard uncertainty based on R_{free} .

^h B -factors from the model refined without TLS.

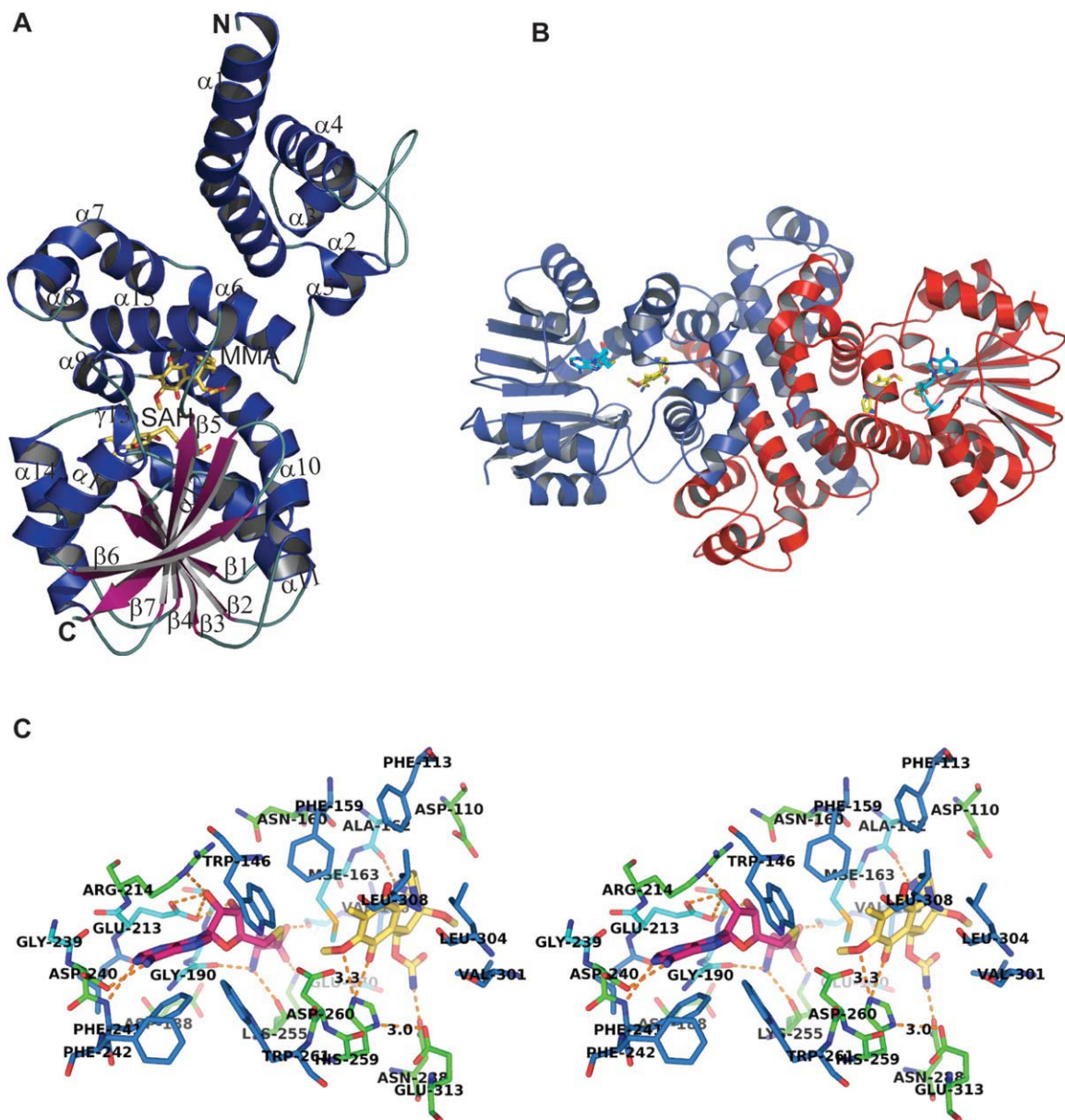


Figure 3

(A) Overview of the secondary structural elements in the MmcR-SAH-MMA ternary complex (helices are colored blue, strands are colored magenta, ligands SAH and MMA are colored yellow, letters N and C correspond to the N-terminus and C-terminus of the MmcR protein, respectively). (B) Ribbon representation of MmcR-SAH-MMA ternary complex quaternary structure, showing dimer interfaces. In this representation, the two monomers are colored red and blue and ligands SAH and MMA are colored cyan and yellow, respectively. (C) Stereoview of interaction of SAH and MMA in MmcR-SAH-MMA complex. The stick model of SAH and MMA are depicted in magenta and yellow, respectively. The interacting MmcR residues are labeled and illustrated in blue, green, and cyan for hydrophobic, charged, and neutral residues, respectively. Polar interactions are depicted by orange dashed lines.

(IOMT),³⁹ calicheamicin *O*-methyltransferase (CalO1),⁴⁰ and caffeic acid/5-hydroxyferulic acid 3/5 *o*-methyltransferase (COMT).⁴¹

The SAM/SAH-binding site

In both determined structures, the cofactor product SAH is well defined by electron density [Fig. 2(A)].

MmcR bears a signature motif (DXGXGXG) containing highly conserved residues for the recognition of SAM/SAH and, like all SAM-dependent MTases, contains conserved active site residues to provide a network of hydrogen-bonding interactions [Fig. 3(C)] with the donor and acceptor of the methyl group (see Fig. 4 for sequence alignment with representative homologs). The carboxylate group of SAH forms an electrostatic inter-

Structural comparison of the MmcR-SAH complex and MmcR-SAH-MMA ternary complex

The four subunits of complexes of MmcR-SAH and MmcR-SAH-MMA structures align with a r.m.s. deviation of 0.31 for 8785 structurally corresponding atoms. The dimers of MmcR-SAH and the MmcR-SAH-MMA complex align with r.m.s. deviation of 0.28 for 4237 structurally corresponding atoms. These low values indicate no large-scale changes in tertiary and/or quaternary structure to occur on substrate binding. The occupancy of the MMA-binding site by MPD in MmcR-SAH crystal form (i.e., representing a “substrate-bound” form) may partially explain the high degree of similarity between the MmcR-SAH and the MmcR-SAH-MMA structures. The only notable structural variation occurs within the solvent-exposed loops surrounding the product MMA (residues 100–106, 289–294, and 335–342), suggesting subtle loop movements in the context of ligand binding.

Structural homology

A DALI search for MmcR structural homologs in the Protein Data Bank (PDB) database returned several hits. Among those, which displayed the highest *Z*-score were carminomycin 4-*O*-methyltransferase (DnrK),³⁷ neocarzinostatin *O*-methyltransferase (NcsB1),³⁸ aclacinomycin hydroxylase (RdmB),⁴² isoflavone methyltransferase (IOMT),³⁹ and calicheamicin *O*-methyltransferase (CalO1),⁴⁰ with *Z*-scores 37, 36, 34, 33, and 32 respectively. They share ~25–35% overall sequence identity with MmcR. Highest sequence conservation is found among residues associated with SAM-binding—specifically, the loop that interacts with the homocysteine and ribosyl moieties of the SAH situated between β 1 and α 11 (which contains the glycine-rich consensus sequence DXGXGXG) and an acidic residue in loop between β 3 and β 4 (Asp240 in MmcR), which interacts with the exocyclic N6 and ring nitrogen N1 of adenine ring of the cofactor. MmcR gives a r.m.s. deviation of 1.7, 1.9, 2.1, 3.2, and 3.7 Å over 330 C $^{\alpha}$, 321 C $^{\alpha}$, 323 C $^{\alpha}$, 330 C $^{\alpha}$, and 345 C $^{\alpha}$ atoms with DnrK, NcsB1, RdmB, IOMT, and CalO1, respectively, and like these three MTases, MmcR is dimeric and also shares high structural similarity across the dimerization domain. Similar to most methyltransferases,³⁹ His259 and Glu313 are implicated as general acid/base pair [Figs. 3(C) and 4] for MmcR catalysis. Specifically, His259 is within range (3.3 Å) [Fig. 3(C)] to deprotonate the hydroxyl group of 7-desmethyl MMA, whereas Glu313 is within the hydrogen bonding distance (3.0 Å) [Fig. 3(C)] of His259 to potentially constrain and orient the catalytic base. Consistent with a putative acid/base-mechanism for MmcR, divalent metals do not influence MmcR activity.¹⁴

ACKNOWLEDGMENTS

Analytical support was provided by the School of Pharmacy Analytical Instrumentation Center.

REFERENCES

- Hata T, Sugawara R. Mitomycin, a new antibiotic from *Streptomyces*. II. Description of the strain. *J Antibiot* 1956;9:147–151.
- Hata T, Hoshi T, Kanamori K, Matsumae A, Sano Y, Shima T, Sugawara R. Mitomycin, a new antibiotic from *Streptomyces*. I. *J Antibiot Ser A* 1956;9:141–146.
- Wakaki S, Marumo H, Tomioka K, Shimizu G, Kato E, Kamada H, Kudo S, Fujimoto Y. Isolation of new fractions of antitumor mitomycins. *Antibiot Chemother* 1958;8:228–240.
- Begleiter A. Clinical applications of quinone-containing alkylating agents. *Front Biosci* 2000;5:E153–E171.
- Galm U, Hager MH, van Lanen SG, Ju J, Thorson JS, Shen B. Antitumor antibiotics: bleomycin, enediynes, and mitomycin. *Chem Rev* 2005;105:739–758.
- McKeown SR, Coweny RL, Williams KJ. Bioreductive drugs: from concept to clinic. *Clin Oncol (R Coll Radiol)* 2007;19:427–442.
- Rockwell S, Dobrucki IT, Kim EY, Marrison ST, Vu VT. Hypoxia and radiation therapy: past history, ongoing research, and future promise. *Curr Mol Med* 2009;9:442–458.
- Bezanson GS, Vining LC. Studies on the biosynthesis of mitomycin C by *Streptomyces verticillatus*. *Can J Biochem* 1971;49:911–918.
- Anderson MG, Kibby JJ, Rickards RW, Rothschild JM. Biosynthesis of the mitomycin antibiotics from 3-amino-5-hydroxybenzoic acid. *J Chem Soc Chem Commun* 1980;1980:1277–1278.
- Hornemann U, Eggert JH. Utilization of the intact carbamoyl group of L-(NH₂CO-¹³C,¹⁵N) citrulline in mitomycin biosynthesis by *Streptomyces verticillatus*. *J Antibiot (Tokyo)* 1975;10:841–843.
- Hornemann Y, Kehler JP, Nunez CS, Ranieri RL. D-glucosamine and L-citrulline, precursors in mitomycin biosynthesis by *Streptomyces verticillatus*. *J Am Chem Soc* 1974;96:320–322.
- Mao Y, Varoglu M, Sherman DH. Molecular characterization and analysis of the biosynthetic gene cluster for the antitumor antibiotic mitomycin C from *Streptomyces lavendulae* NRRL 2564. *Chem Biol* 1999;6:251–263.
- Sitachitta N, Lopanik NB, Mao Y, Sherman DH. Analysis of a parallel branch in the mitomycin biosynthetic pathway involving the mitN-encoded aziridine *N*-methyltransferase. *J Biol Chem* 2007;282:20941–20947.
- Gruschow S, Chang LC, Mao Y, Sherman DH. Hydroxyquinone *O*-methylation in mitomycin biosynthesis. *J Am Chem Soc* 2007;129:6470–6476.
- Zhang C, Weller RL, Thorson JS, Rajski SR. Natural product diversification using a non-natural cofactor analogue of *S*-adenosyl-L-methionine. *J Am Chem Soc* 2006;128:2760–2761.
- Zhang C, Albermann C, Fu X, Peters NR, Chisholm JD, Zhang G, Gilbert EJ, Wang PG, Van Vranken DL, Thorson JS. RebG- and RebM-catalyzed indolocarbazole diversification. *Chembiochem* 2006;7:795–804.
- Singh S, McCoy JG, Zhang C, Bingman CA, Phillips GN, Jr, Thorson JS. Structure and mechanism of the rebeccamycin sugar 4'-*O*-methyltransferase RebM. *J Biol Chem* 2008;283:22628–22636.
- Lukinavicius G, Lapiene V, Stasevskij Z, Dalhoff C, Weinhold E, Klimasauskas S. Targeted labeling of DNA by methyltransferase-directed transfer of activated groups (mTAG). *J Am Chem Soc* 2007;129:2758–2759.
- Klimasauskas S, Weinhold E. A new tool for biotechnology: AdoMet-dependent methyltransferases. *Trends Biotechnol* 2007;25:99–104.
- Peters W, Willnow S, Duisken M, Kleine H, Macherey T, Duncan KE, Litchfield DW, Lüscher B, Weinhold E. Enzymatic site-specific functionalization of protein methyltransferase substrates with

- alkynes for click labeling. *Angew Chem Int Ed Engl* 2010;49:5170–5173.
21. Dalhoff C, Lukinavicius G, Klimasauskas S, Weinhold E. Synthesis of *S*-adenosyl-L-methionine analogs and their use for sequence-specific transalkylation of DNA by methyltransferases. *Nat Protoc* 2006;1:1879–1886.
 22. Dalhoff C, Lukinavicius G, Klimasauskas S, Weinhold E. Direct transfer of extended groups from synthetic cofactors by DNA methyltransferases. *Nat Chem Biol* 2006;2:31–32.
 23. Sreenath HK, Bingman CA, Buchan BW, Seder KD, Burns BT, Geetha HV, Jeon WB, Vojtik FC, Aceti DJ, Frederick RO, Phillips GN, Jr, Fox BG. Protocols for production of selenomethionine-labeled proteins in 2-L polyethylene terephthalate bottles using auto-induction medium. *Protein Expr Purif* 2005;40:256–267.
 24. Otwinowski Z, Minor W. Processing of X-ray diffraction data collected in oscillation mode. *Methods Enzymol* 1997;276:307–326.
 25. Grosse-Kunstleve RW, Adams PD. Substructure search procedures for macromolecular structures. *Acta Crystallogr Sect D* 2003;59:1966–1973.
 26. Schneider TR, Sheldrick GM. Substructure solution with SHELXD. *Acta Crystallogr Sect D* 2002;58:1772–1779.
 27. Dall'Antonia F, Baker PJ, Schneider TR. Optimization of selenium substructures as obtained from SHELXD. *Acta Crystallogr Sect D* 2003;59:1987–1994.
 28. de la Fortelle E, Bricogne G. Maximum-likelihood heavy-atom parameter refinement for multiple isomorphous replacement and multiwavelength anomalous diffraction methods. *Methods Enzymol* 1997;276:472–494.
 29. Perrakis A, Morris R, Lamzin VS. Automated protein model building combined with iterative structure refinement. *Nat Struct Biol* 1999;6:458–463.
 30. Vagin A, Teplyakov A. MOLREP: an automated program for molecular replacement. *J Appl Crystallogr* 1997;30:1022–1025.
 31. Emsley P, Cowtan K. Coot: model-building tools for molecular graphics. *Acta Crystallogr Sect D* 2004;60:2126–2132.
 32. Murshudov GN, Vagin AA, Dodson EJ. Refinement of macromolecular structures by the maximum-likelihood method. *Acta Crystallogr Sect D* 1997;53:240–255.
 33. Adams PD, Grosse-Kunstleve RW, Hung LW, Ioerger TR, McCoy AJ, Moriarty NW, Read RJ, Sacchettini JC, Sauter NK, Terwilliger TC, PHENIX: building new software for automated crystallographic structure determination. *Acta Crystallogr Sect D* 2002;58:1948–1954.
 34. Davis IW, Leaver-Fay A, Chen VB, Block JN, Kapral GJ, Wang X, Murray LW, Arendall WB, III, Snoeyink J, Richardson JS, Richardson DC. MolProbity: all-atom contacts and structure validation for proteins and nucleic acids. *Nucleic Acids Res* 2007;35:W375–W383.
 35. Laskowski RA, Rullmann JA, MacArthur MW, Kaptein R, Thornton JM. AQUA and PROCHECK-NMR: programs for checking the quality of protein structures solved by NMR. *J Biomol NMR* 1996;8:477–486.
 36. Potterton E, Briggs P, Turkenburg M, Dodson EA. Graphical user interface to the CCP4 program suite. *Acta Crystallogr D Biol Crystallogr* 2003;59:1131–1137.
 37. Jansson A, Koskiniemi H, Mantsala P, Niemi J, Schneider G. Crystal structure of a ternary complex of DnrK, a methyltransferase in daunorubicin biosynthesis, with bound products. *J Biol Chem* 2004;279:41149–41156.
 38. Cooke HA, Guenther EL, Luo Y, Shen B, Bruner SD. Molecular basis of substrate promiscuity for the SAM-dependent *O*-methyltransferase NcsB1, involved in the biosynthesis of the enediyne antitumor antibiotic neocarzinostatin. *Biochemistry* 2009;48:9590–9598.
 39. Zubieta C, He XZ, Dixon RA, Noel JP. Structures of two natural product methyltransferases reveal the basis for substrate specificity in plant *O*-methyltransferases. *Nat Struct Mol Biol* 2001;8:271–279.
 40. Chang A, Singh S, Bingman CA, Thorson JS, Phillips Jr GN. Structural characterization of CalO1: A putative orsellinic acid methyltransferase in the calicheamicin biosynthetic pathway. *Acta Cryst D* 2011; D67:197–203.
 41. Palma PN, Rodrigues ML, Archer M, Bonifácio MJ, Loureiro AI, Learmonth DA, Carrondo MA, Soares-da-Silva P. Comparative study of ortho- and meta-nitrated inhibitors of catechol-*O*-methyltransferase: interactions with the active site and regioselectivity of *O*-methylation. *Mol Pharmacol* 2006;70:143–153.
 42. Jansson A, Niemi J, Lindqvist Y, Mantsala P, Schneider G. Crystal structure of aclacinomycin-10-hydroxylase, a *S*-adenosyl-L-methionine-dependent methyltransferase homolog involved in anthracycline biosynthesis in *Streptomyces purpurascens*. *J Mol Biol* 2003; 334:269–280.